25th ABCM International Congress of Mechanical Engineering
October 20-25, 2019, Uberlândia, MG, Brazil

COB-2019-1424
NUMERICAL SIMULATION OF NON-ISOTHERMAL FLOW IN NATURALLY FRACTURED OIL RESERVOIRS USING A ONE-EQUATION MODEL

Juan Diego dos Santos Heringer
Paulo de Tarço Honório Jr.
Grazione de Souza
Helio Pedro Amaral Souto
Polytechnic Institute, Rio de Janeiro State University, Nova Friburgo, Brazil
jheringer21@gmail.com; ptarco@iprj.uerj.br; gsouza@iprj.uerj.br; helio@iprj.uerj.br

Abstract. *This work aims to simulate three-dimensional heavy oil flow in a naturally fractured reservoir with heater-wells. When simulating oil reservoirs, the heterogeneities have significant relevance in the dynamics of the flow. Naturally fractured reservoirs (NFRs), for example, may have different temperature and pressure settings, depending on the permeability and porosity fields. In this work, mass, momentum and energy balances, as well as correlations for rock and fluid properties, are used to obtain the non-linear partial differential equations for the fluid pressure and fluid and rock temperatures. The governing equations are then discretized using the Finite Volume Method (FVM) and solved along with linearization and an operator splitting. As a consequence, three subsystems of linearized algebraic equations arise and are solved using two different methods, the Conjugate Gradient Method and Preconditioned Conjugate Gradient Method. We also use a grid refinement around the wellbores and the fractures to better represent the physical phenomena in those regions. The results obtained with the governing equations for the fluid flow and the one-equation model for the heat transfer show the suitability of heater-wells application in naturally fractured reservoirs.*

Keywords: *Finite volume method, heavy oil, naturally fractured reservoir, non-isothermal flow*

1. INTRODUCTION

For many years, the simulation of fluid flow and heat transfer in natural porous media has attracted the attention of geoscientists and mathematicians (Mezon *et al.*, 2018). Moreover, the growing threat of a global energy crisis, which had begun in the 1970s, has stimulated research on renewable energies and on the use of new techniques to enhance the hydrocarbon recovery. Since then, scientists and engineers have focused their attention to mathematical and numerical strategies to solve problems related to reservoir engineering. In this sense, realistic numerical simulation is of great importance for many applications such as in the oil industry and geothermal energy, to mention a few.

Petroleum reservoir is a porous media containing rock and fluids such as gas and oil. In general, we can say that all reservoirs have fractures to some extent. Fractures occur in response to stress, and the source of such stress may originate from several processes. These fractures often have higher permeability values when compared to the other regions of the reservoir and, as well know, the fluid tends to flow preferably through the paths that offer less resistance. Furthermore, we find a fraction of the world's water and energy resources in naturally fractured reservoirs within the earth's crust (Jansen, 2018). Therefore, the understanding of the fluid flow behavior through the fractures is of significant importance in geotechnical engineering and reservoir simulation, since many petroleum, gas, geothermal, and water supply reservoirs are formed by fractured rocks (Dyrdah, 2014).

Among the phenomena that take place in the reservoir, we can highlight the heat transfer. For example, the geothermal gradient plays a significant role in reservoir fluid properties. So, disregarding its effect might result in an error in the forecast of oil production, mainly for reservoirs that can show significant variations in temperature with depth (Safari *et al.*, 2017). Taking into account the existence of fractures in heavy-oil reservoirs also makes reservoir simulation more realistic. The challenge of the numerical simulation of these reservoirs is due to the nature of the rock with its geological and rock-fluid properties complexity (Ezeuko and Gates, 2018), in a scenario of preferential paths for the fluid flow.

Enhanced oil recovery (EOR), or tertiary recovery, is commonly applied to extract an extra amount of oil from the reservoir after the primary (production based on reservoir energy) and secondary (immiscible fluid injection) recoveries. EOR techniques include chemical, miscible displacement, biological and thermal methods (Manichand, 2002), increasing the recovery of hydrocarbons by changing the properties of the fluid. Static heaters, for instance, include different me-

chanical structures (such as an antenna), based on microwave or electricity. The heaters are supposed to transfer thermal energy to a specific region of the reservoir to warm-up both rock and fluid. Some authors focus their attention on the financial reliability of the process of adding heat to specific regions in the reservoir like in Liu *et al.* (2019). However, in this work, we only consider the physical effects.

In this context, this work deals with the numerical simulation of the non-isothermal three-dimensional flow of heavy oil in a naturally fractured reservoir containing static heaters. Therefore, we take into account the geothermal gradient, and we give special attention to the fractured regions. Mass, momentum and energy balances, as well as relations for the determination of rock and fluid physical properties, are used to obtain the governing nonlinear partial differential equations. Next, suitable numerical methods (Finite Volume and Preconditioned Conjugate Gradient) are used to determine the unknowns fluid pressure and temperature.

2. PHYSICAL-MATHEMATICAL MODELING

Mainly two types of fractures have been studied for scientists and engineers, production wells artificially fractured and naturally fractured reservoirs. The first refers to a method used to enhance oil production, removing the formation damage or even intensifying the hydrocarbon flow. Also, in this type of technique, the fissures can be created by either acidification or hydraulic cracking. In this work, we focus on heterogeneities formed by nature (Rosa *et al.*, 2006) (the second type).

Over time several conceptual models have been developed for describing fluid flow in fractured porous media. The methods differ in how they model storage and flow capabilities of the porous medium and the fracture (Dyrdah, 2014): equivalent continuum model, dual-porosity model, multiple interacting continua model, dual-porosity dual-permeability model, and discrete fracture model (de Souza and Souto, 2014). The last one is used by the authors to model the flow into the naturally fractured reservoir. In discrete fracture models, we place each fracture explicitly in the numerical grid, and we treat the system as any other non-homogeneous medium (Lampe, 2013).

Here, as in de Souza and Souto (2014), the fractures do not form a continuous conductive network, so we represent only a few fractures but, in this case, without hydraulic communication with each other. We can consider the fractures as being heterogeneous regions inside the reservoir having different values of permeability and porosity. Each fracture has an aperture size and, with this value, it is possible to establish the logarithmic refinement of the grid to be used. This is necessary because of the disparity in the length scales associated with the reservoir (km) and fractures (cm) (Praditia *et al.*, 2018).

2.1 Governing equations

We obtain temperature and pressure distribution in the reservoir from the resolution of the equations governing the flow and the transfer of energy. We establish these macroscopic equations from mass, momentum, and energy balance postulates. Therefore, the equation that describes the mass balance, in terms of the formation-volume-factor (FVF), is given by (Ertekin *et al.*, 2001)

$$\frac{\partial}{\partial t}\left(\frac{\phi}{B}\right) - \nabla \cdot \left(\frac{\mathbf{v}}{B}\right) - \frac{q_{sc}}{V_b} = 0, \tag{1}$$

where ϕ and B are the porosity and the FVF, respectively, q_{sc} represents a source term in standard conditions, V_b is the total volume, and the apparent velocity is represented by the vector $\mathbf{v}$, which is provided by the Darcy's law (momentum balance) (Ertekin *et al.*, 2001)

$$\mathbf{v} = -\frac{\mathbf{k}}{\mu}\left(\nabla p - \rho g \nabla D\right), \tag{2}$$

where $\mathbf{k}$ is the permeability tensor, p is the pressure in the reservoir, ρ is the fluid density, g the magnitude of gravity, D the depth, and μ is the fluid viscosity. This last parameter depends on temperature and is calculated by (Heringer *et al.*, 2019)

$$\mu = a \exp\left(\frac{b}{T - T_{ref,\mu}}\right) \tag{3}$$

where a, b and $T_{ref,\mu}$ must be provided.

We also consider that the porosity and the formation-volume-factor are functions of pressure and temperature such as (Heringer *et al.*, 2019)

$$\phi(p, T_r) = \phi^0 \left[1 + c_\phi \left(p - p^0\right) - c_{\phi T}\left(T_r - T_r^0\right)\right], \tag{4}$$

and

$$B(p, T_f) = \frac{B^0}{1 + c_o\left(p - p^0\right) - c_{oT}\left(T_f - T_f^0\right)}. \tag{5}$$

where T_r and T_f represent respectively rock and fluid temperatures, with c_o and c_ϕ being the compressibilities of the fluid and rock respectively. From Eqs. (4) and Eq. (5) we see that porosity is directly proportional while FVF is inversely proportional to the temperature.

Now, taking the partial derivative of ϕ with respect to p and T_r, and of B with respect to p and T_f, and after reordering the terms, we obtain from Eq. (1) (Lampe, 2013)

$$\Gamma_p \frac{\partial p}{\partial t} - \Gamma_{T_r} \frac{\partial T_r}{\partial t} - \Gamma_{T_f} \frac{\partial T_f}{\partial t} + \nabla \cdot \left(\frac{\mathbf{v}}{B}\right) - \frac{q_{sc}}{V_b} = 0 \tag{6}$$

where

$$\Gamma_p = \left(\frac{\phi c_o}{B^0} + \frac{\phi^0 c_\phi}{B}\right), \quad \Gamma_{T_r} = \left(\frac{\phi^0 c_{\phi T}}{B}\right) \quad \text{and} \quad \Gamma_{T_f} = \left(\frac{\phi c_{oT}}{B^0}\right), \tag{7}$$

with c_{oT} and $c_{\phi T}$ representing respectively the thermal expansion coefficients of both phases (fluid and rock), and the superscript "o" stands for the reference values.

In our development, we do not assume the hypotheses of local thermal equilibrium. Even so, there are two forms to describe the heat transfer, as point out by Heringer *et al.* (2019), using a one- or two-equation models. Nevertheless, for some range of thermal properties, both models provide correct results Heringer *et al.* (2019), and this applies to the case studied in this work. Given this fact, and bearing in mind that the two-equation model demands a greater computational effort, we use here only the one-equation model to simulate the heat transfer in the porous media. Then, we introduce an average temperature (for the reservoir) obtained from the fluid and rock temperatures (Moyne *et al.*, 2000):

$$\overline{\rho c_p}\, T = \phi \rho_f c_{p_f} T_f + (1 - \phi) \rho_r c_{p_r} T_r \tag{8}$$

where $\overline{\rho c_p} = \phi \rho_f c_{p_f} + (1 - \phi) \rho_r c_{p_r}$ is the average heat capacity of the reservoir, and the energy equation is given by (Moyne *et al.*, 2000)

$$\frac{\partial}{\partial t}(\overline{\rho c_p}\, T) + \nabla \cdot (\rho_f h_f \mathbf{v}) - \nabla \cdot (\mathbf{K} \nabla T) - \frac{q_H}{V_b} - \frac{\rho_f h_f q_{sc}}{V_b} = 0 \tag{9}$$

where the subscripts r and f denote rock and fluid, c_{pf} and c_{pr} are the specific heats of rock and fluid, $h_f = c_{pf} T_f$ is the fluid enthalpy, and $\mathbf{K}$ represents the effective thermal dispersion tensor (we consider only the contribution due to the thermal conductivity). The source term q_H / V_b represents the increase or decrease of heat in the reservoir due to the heaters, and $\rho_f h_f q_{sc} / V_b$ represents the gain or loss of energy related to injection or extraction of fluid into or from the reservoir.

Having introduced both mass and energy balance, it is necessary now to solve those non-linear partial differential equations for the particular problem established. This set of differential equations is solved using the Finite Volume Method along with linearization, operator splitting, and Conjugate Gradient methods (Heringer *et al.*, 2019).

2.2 Initial and boundary conditions

As initial conditions, according to to Safari *et al.* (2017), a linear relation is used to impose the temperature value for oil and rock everywhere in the reservoir,

$$T = \nabla T\big|_0 D + 330.0 \tag{10}$$

where $\nabla T\big|_0$ is the initial temperature gradient (equal to 0.03 K/m), D is the depth, and T is the temperature at some point in space.

We set a pre-established value for the oil pressure (for a given depth) according to the hydrostatic gradient. Also, there is neither mass flow nor energy transfer across the external boundaries of the reservoir so that we use Neumann boundary conditions to represent null flux.

3. Numerical solution methodology

The Finite Volume Method is a conservative numerical method for solving partial differential equations based on a volume integral formulation (Leveque, 2004). The domain is partitioned using a finite volume set (elements or cells)

(Moukalled *et al.*, 2016), and in this work, we use a structured mesh. In our case, the discretized partial differential equations give rise to a system of coupled non-linear algebraic equations.

The domain is filled by finite cubic volumes, as shown in Fig. 1, and the faces of the finite volumes are represented by: $i-1/2, j, k = w$, $i+1/2, j, k = e$, $i, j-1/2, k = n$, $i, j+1/2, k = s$, $i, j, k-1/2 = b$ and $i, j, k+1/2 = a$, where w, e, n, s, b and a stand for *west, east, north, south, below* and *above*. The center of the cell is $P(i, j, k)$, and the neighbors are represented by: $i-1, j, k = W$, $i-1, j, k = E$, $i, j-1, k = N$, $i, j+1, k = S$, $i, j, k-1 = A$, and $i, j, k+1 = B$.

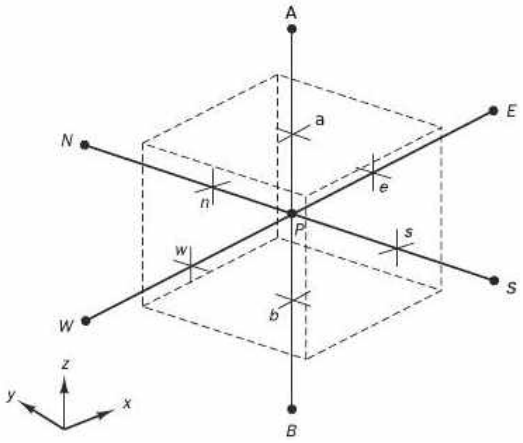

Figure 1. Finite volume and its neighbors.

Once we have discretized the domain, we integrate over time and space (over a finite volume) the conservative form of the non-linear partial differential equations. After integration, we use central differences to approximate the first-order spatial derivatives. Finally, the discretized equations for pressure and temperature contain geometrical and transmissibility terms, which must be determined on the interface of the finite volumes, as described by Heringer *et al.* (2019).

3.1 Linearization and operator splitting

As already seen, the discretized equations form a system of non-linear algebraic equations which must be solved numerically. The numerical solution strategy for the single-phase non-isothermal flow considered here predicts the calculation of each equation separately, applying an operator splitting (Dyrdah, 2014) and a Picard linearization procedure.

The linearization procedure plays an important role. Thanks to it, we can evaluate the nonlinear coefficients in the previous iteration level. When the calculation starts, for each time step, the values of p and T are estimated in an iterative level v and time $n+1$. Next, fluid and rock properties are updated, and the pressure is calculated from the known value $T^{n+1,v}$ obtained in the previous iteration. Finally, we use $p^{n+1,v+1}$, recently calculated, to update the temperature by solving the corresponding equation, and we update all physical properties from the new values of $p^{n+1,v+1}$ and $T^{n+1,v+1}$.

The main advantage of the splitting method is the reduction of the number of calculations required for each time step. For instance, if there are N finite volumes, and we want to solve the coupled system using a fully implicit scheme, we must solve $4N^2$ equations. Differently, for the uncoupled system, it can be reduced to $2N^2$ algebraic equations. However, it still will demand a lot of computer memory, and the computation time might be excessive (Vennemo, 2016).

Hence, we are concerned with the numerical solution of two subsystems of linear algebraic equations, one for the pressure and one for the temperature. Thus, for the pressure equation, we have (Heringer *et al.*, 2019)

$$\Phi_x\Big|^{n+1,v}_{i-1/2,j,k} p^{n+1,v+1}_{i-1,j,k} + \Phi_y\Big|^{n+1,v}_{i,j-1/2,k} p^{n+1,v+1}_{i,j-1,k} + \Phi_z\Big|^{n+1,v}_{i,j,k-1/2} p^{n+1,v+1}_{i,j,k-1}$$

$$+\Phi_x\Big|^{n+1,v}_{i+1/2,j,k} p^{n+1,v+1}_{i+1,j,k} + \Phi_y\Big|^{n+1,v}_{i,j+1/2,k} p^{n+1,v+1}_{i,j+1,k} + \Phi_z\Big|^{n+1,v}_{i,j,k+1/2} p^{n+1,v+1}_{i,j,k+1}$$

$$-\left[\overline{\Phi}^{n+1,v}_{x,y,z} + \frac{(\Gamma_p)^{n+1,v}_{i,j,k}}{\Delta t}\right] p^{n+1,v+1}_{i,j,k} = \frac{(\Gamma_p)^{n+1,v}_{i,j,k}}{\Delta t} p^{n}_{i,j,k} + \frac{(\Gamma_T)^{n+1,v}_{i,j,k}}{\Delta t}\left[(T)^{n+1,v}_{i,j,k} - (T)^{n}_{i,j,k}\right]$$

$$-(\Omega_z)^{n+1,v}_{i,j,k+1/2}(D_{i,j,k+1} - D_{i,j,k}) + (\Omega_z)^{n+1,v}_{i,j,k-1/2}(D_{i,j,k} - D_{i,j,k-1}) - q^{n+1}_{sc,i,j,k} \tag{11}$$

where the transmissibility terms (for x-direction) are defined as:

$$(\Phi_x)\Big|_e = \left(\frac{A_x k_x}{\mu B \Delta x}\right)_e, \qquad (\Phi_x)\Big|_w = \left(\frac{A_x k_x}{\mu B \Delta x}\right)_w, \tag{12}$$

while for the hydrostatic terms we have

$$(\Omega_z)\Big|_a = \left(\frac{A_z k_z \rho_f g}{\mu B \Delta z}\right)_a, \qquad (\Omega_z)\Big|_b = \left(\frac{A_z k_z \rho_f g}{\mu B \Delta z}\right)_b, \tag{13}$$

and,

$$\overline{\Phi}^{n+1,v}_{x,y,z} = \Phi_x\Big|^{n+1,v}_{i+1/2,j,k} + \Phi_x\Big|^{n+1,v}_{i-1/2,j,k} + \Phi_x\Big|^{n+1,v}_{i,j+1/2,k} + \Phi_x\Big|^{n+1,v}_{i,j-1/2,k} + \Phi_x\Big|^{n+1,v}_{i,j,k+1/2} + \Phi_x\Big|^{n+1,v}_{i,j,k-1/2}. \tag{14}$$

For the temperature of the fluid, the following equation is considered (Heringer *et al.*, 2019):

$$\begin{aligned}
&(\Lambda_f)_x\Big|_{i-1/2,j,k} T^{n+1,v+1}_{i-1,j,k} + (\Lambda_f)_y\Big|_{i,j-1/2,k} T^{n+1,v+1}_{i,j-1,k} + (\Lambda_f)_z\Big|_{i,j,k-1/2} T^{n+1,v+1}_{i,j,k-1} \\
&+(\Lambda_f)_x\Big|_{i+1/2,j,k} T^{n+1,v+1}_{i+1,j,k} + (\Lambda_f)_y\Big|_{i,j+1/2,k} T^{n+1,v+1}_{i,j+1,k} + (\Lambda_f)_z\Big|_{i,j,k+1/2} T^{n+1,v+1}_{i,j,k+1} \\
&- \left[(\overline{\Lambda}_f)_{x,y,z} + V_b AH + V_b \left(\frac{\rho c_{cp}}{\Delta t}\right)^{n+1,v}_{i,j,k}\right] T^{n+1,v+1}_{i,j,k} = -V_b \left(\frac{\rho c_{cp}}{\Delta t}\right)^{n+1,v}_{i,j,k} T^{n}_{i,j,k} \\
&+(\Psi_z)^{n+1,v}_{i,j,k+1/2}(D_{i,j,k+1} - D_{i,j,k}) - (\Psi_z)^{n+1,v}_{i,j,k-1/2}(D_{i,j,k} - D_{i,j,k+1}) \\
&+\overline{\Theta}^{n+1,v}_{x,y,z} - (\rho_f h q_{sc})^{n+1}_{i,j,k} - q_H\Big|^{n+1}_{i,j,k}.
\end{aligned} \tag{15}$$

and for the energy equations, we introduce

$$(\Lambda)\Big|_w = \left(\frac{A_x(\kappa)_x}{\Delta x}\right)_w, \qquad (\Lambda)\Big|_e = \left(\frac{A_x(\kappa_x}{\Delta x}\right)_e \tag{16}$$

and

$$(\Psi_z)\Big|_a = \left(\frac{A_z \rho_f h g k_z}{\mu \Delta z}\right)_a, \qquad (\Psi_z)\Big|_b = \left(\frac{A_z \rho_f h g k_z}{\mu \Delta z}\right)_b. \tag{17}$$

where

$$\begin{aligned}
\frac{\overline{\Theta}_{x,y,z}}{\rho_{fsc}} &= (h\Phi_x)^{n+1}_{i-1/2,j,k}(p_{i,j,k} - p_{i-1,j,k})^{n+1} - (h\Phi_x)^{n+1}_{i+1/2,j,k}(p_{i+1,j,k} - p_{i,j,k})^{n+1} \\
&+ (h\Phi_y)^{n+1}_{i,j-1/2,k}(p_{i,j,k} - p_{i,j-1,k})^{n+1} - (h\Phi_y)^{n+1}_{i,j+1/2,k}(p_{i,j+1,k} - p_{i,j,k})^{n+1} \\
&+ (h\Phi_z)^{n+1}_{i,j,k-1/2}(p_{i,j,k} - p_{i,j,k-1})^{n+1} - (h\Phi_z)^{n+1}_{i,j,k+1/2}(p_{i,j,k+1} - p_{i,j,k})^{n+1},
\end{aligned} \tag{18}$$

and

$$\begin{aligned}
(\overline{\Lambda}_f)_{x,y,z} &= (\Lambda_f)_x\Big|_{i,j+1/2,k} + (\Lambda_f)_x\Big|_{i-1/2,j,k} + (\Lambda_f)_y\Big|_{i,j+1/2,k} \\
&+ (\Lambda_f)_y\Big|_{i,j-1/2,k} + (\Lambda_f)_z\Big|_{i,j,k+1/2} + (\Lambda_f)_z\Big|_{i,j,k-1/2}.
\end{aligned} \tag{19}$$

3.2 Numerical solution of the linear systems

The last step of the FVM consists of the solution of the set of algebraic equations, Eqs. (11) and (15). Here we chose the Conjugate Gradient Method, a well known and efficient iterative algorithm, to solve the two subsystems of linearized equations (Ertekin *et al.*, 2001), knowing that the coefficient matrices are symmetric. As usual, we can put the system structure in the following form:

$$\mathbf{A}\mathbf{x} = \mathbf{d} \tag{20}$$

where $\mathbf{A}$ is the coefficient matrix, $\mathbf{x}$ is the unknown vector, and $\mathbf{d}$ is the vector of the known values.

As is well known, we can improve the CG method by reducing the condition number of the coefficient matrix (the ratio between the largest and the smallest eigenvalue of the matrix) to a value close to one. One way to do this is to use a preconditioning scheme, such that we reduce the spectral radius of the coefficient matrix.

There are various algorithms for preconditioning, one of them, is the diagonal preconditioning or Point Jacobi Preconditioner. In this case, the preconditioned matrix $\mathbf{P}$ is diagonal, and it contains the diagonal elements of the matrix $\mathbf{A}$. We make null all the elements off the diagonal. Then, the original system is rewritten as

$$\mathbf{A}_p\mathbf{y} = \mathbf{d} \tag{21}$$

where $\mathbf{A}_p = \mathbf{A}\mathbf{P}^{-1}$ and, $\mathbf{y} = \mathbf{P}\mathbf{x}$.

This method can bring significant improvement when compared to the CG method without preconditioning, even though it is one of the simplest. The gain in computational efficiency is even more relevant when using a mesh refinement, which tends to increase execution time.

4. NUMERICAL RESULTS

A series of tests were performed to investigate the effect of fractures, heterogeneities, and static heaters in heavy oil reservoir production. We considered in all simulations a reservoir with four static heaters, four planar fractures, and one vertical producer well, placed in the z-direction in the center of the reservoir.

In Tab. 1 we find the properties of the matrix (porosity, ϕ_{init}, and permeability, k_x, k_y, and k_y), distance from each heater to the well (L_T), the lengths (L_x, L_y, and L_z) of the reservoir, the flow rate ($Q_{sc} = \sum q_{sc}$), and the electric power of the heaters ($Q_H = \sum q_H$).

Table 1. Parameters for the reservoir

Parameter	Unit	Value	Parameter	Unit	Value
$\phi_{init} = \phi^0$	-	0.3	L_y	m	1,840
$k_x = k_y = k_z$	m^2	1.0 10^{-15}	L_z	m	120
L_T	m	40	Q_{sc}	STB/day	-10.0
L_x	m	1,840	Q_H	kW	320

We have four fractures in the xz-plane, and we show their properties in the Tab. 2. Where we have the porosity (ϕ_f), the permeability (k_f), the position of the fractures in the y direction, y_f, the aperture, l_y, and also the length and width, $l_x(m)$ and $l_z(m)$, respectively.

Table 2. Characteristics of fractures.

Fracture	ϕ_f	k_f (mD)	y_f (m)	l_y (m)	l_x (m)	l_z (m)
1	0.8	2.0	830	0.4	300	10
2	0.6	1.0	870	0.2	300	10
3	0.8	3.0	960	0.4	100	10
4	0.8	4.0	970	0.4	300	10

Other important parameters are given in Tab. 3: initial time step (Δt_{init}), final time step (Δt_{max}), time step increase rate (F_{Δ_t}), maximum simulation time (t_{max}), initial pressure (P_{init}), initial temperatures for fluid ($T_{f_{ini}}$) and rock ($T_{r_{ini}}$), and the number of cells (n_x, n_y and n_z) in the three spatial directions. We choose the mesh according to the mesh refinement study carried out by Heringer *et al.* (2019).

Table 4 presents the properties with respect to the oil: standard (p_{sc}) and reference (p^0) pressures, standard temperature (T_{sc}), reference temperature (T_{ref_μ}) to determine the fluid viscosity, density (ρ^0) and formation-volume-factor of reference (B^0), a and b parameters for Eq. (3), coefficient of compressibility (c_f), coefficient of thermal expansion (c_{fT}), heat capacity (c_{pf}), and thermal conductivity (κ_f).

Table 3. Parameters for the numerical simulation

Parameter	Unit	Value	Parameter	Unit	Value
Δt_{init}	day	1.0 10^{-1}	$T_{r_{ini}}$	K	330
Δt_{max}	day	1.0	$T_{f_{ini}}$	K	330
F_{Δ_t}	-	1.1	n_x	-	185
t_{max}	day	600	n_y	-	185
P_{init}	kPa	1.0 10^4	n_z	-	9

Table 4. Fluid Properties

Parameter	Unit	Value	Parameter	Unit	Value
p_{sc}	kPa	101.3 10^3	a	Pa.s	3.0 10^{-4}
p^0	kPa	69 10^3	b	K	333.33
T_{sc}	K	277.78	c_f	kPa^{-1}	6.25 10^{-7}
T_{ref_μ}	K	277.7	c_{fT}	K $^{-1}$	9.2 10^{-4}
ρ^0	kg/m ^{3}	1,034	c_{pf}	J/kg.K ^{3}	2,100
B^0	RB/STB	1.3	κ_f	W/m K	0.1225

Lastly, the properties of the rock are shown in Tab. 5: density (ρ_r), superficial specific area of the fluid-rock interface (A), heat capacity (c_{pr}), coefficient of compressibility (c_r), coefficient of thermal expansion (c_{rT}), and thermal conductivity (κ_r).

Table 5. Rock properties

Parameter	Unit	Value	Parameter	Unit	Value
ρ_r	kg/m ^{3}	2,500	c_r	kPa^{-1}	3.35 10^{-7}
A	m $^{-1}$	200	c_{rT}	K $^{-1}$	1.8 10^{-3}
c_{pr}	J/kg.K	1,200	κ_r	W/m K	4.5

Two cases were carried out initially, one using the Conjugate Gradient method and another the Preconditioned Conjugate Gradient (PCG). We solved the same problem, for a maximum simulation time equal to 10 days, except for the use of the iterative method with and without preconditioning. Due to the reduction of the spectral radius of the coefficient matrix, we achieved the computational times show in Tab. 6. We can observe, without a doubt, the gain when using preconditioning. We performed the calculations on a Dell PowerEdge R720 with an Intel Xeon E5-2620 processor.

Table 6. Execution time for CG and PCG methods.

Solver	Execution Time (s)
Without preconditioning (CG)	26,864
With preconditioning (PCG)	3,803

Moreover, we compared both pressure and temperature obtained with CG and PCG methods. As can be seen in Fig. 2, the same values are determined regardless of the solver used.

In Fig. 3(a) it is possible to see the pressure distribution over the heavy oil reservoir, on the xz-plane, as a cross section area, and in Fig. 3(b) on the xy-plane seen from the top.

In these two figures, we can realize that there is a pressure reduction near the production well and that the pressure is higher at the bottom than at the top. Moreover, we can say that the pressure reduction is sharper at the top than at the bottom. Near the fractures, there is also a significant change in pressure. Pressure drops more rapidly in the fractures since the fluid flows with higher velocity as a consequence of the different porosity and permeability values in comparison with the rest of the reservoir, and it is also possible to see the appearance of preferential paths.

Furthermore, as we can observe in Figure 3, in the neighborhood of the producer well, the pressure is changing in the positions corresponding to the four static heaters. This is due to the increase in fluid temperature.

In Fig. 4, we have a corresponding temperature distribution. We see that the temperature is higher at the bottom due to the geothermal effect, and in the neighborhood of the heaters, the temperature is increasing. In the regions near the fractures and the producer well, we can notice a decrease in temperature. We already expected this result due to the increase of fluid mobility in the fractures, leading to higher advective transport and, as a consequence, the producer well receives more energy.

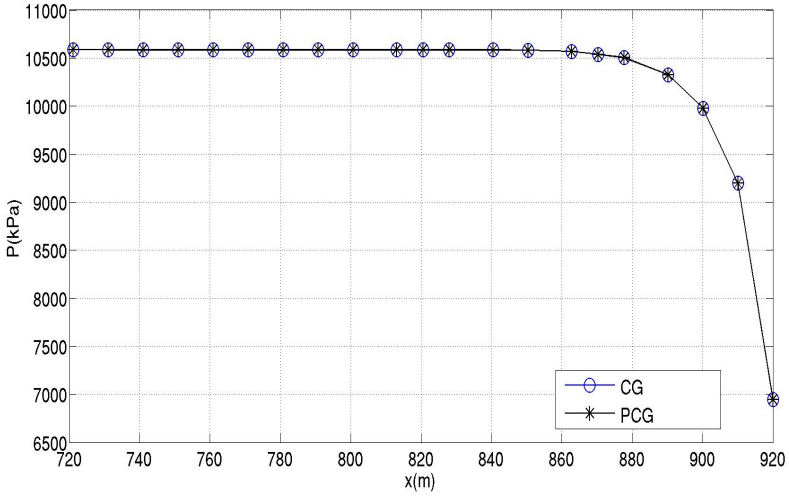

(a) Pressure determined with CG and PCG methods.

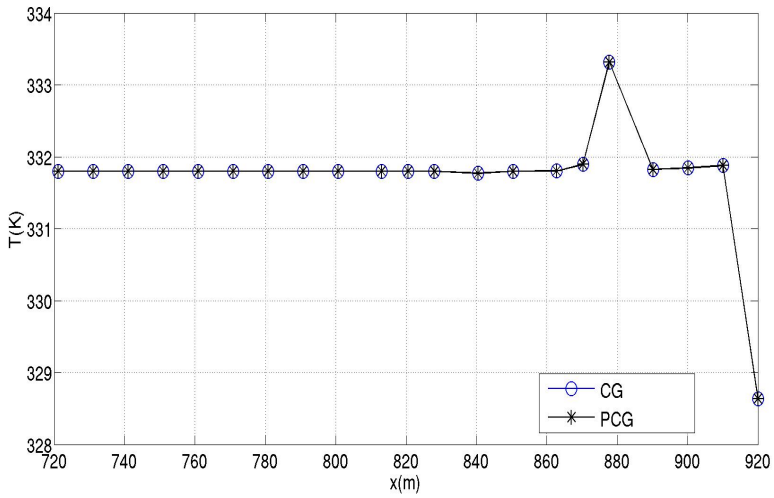

(b) Temperature determined with CG and PCG methods.

Figure 2. Pressure and temperature profiles for t_{max} equal to 10 days and fixed values of y and z.

5. CONCLUSION

In this work, we simulated a heavy oil flow in a reservoir containing a vertical producer well, four fractures, and four static heaters. The authors used the Discrete Fracture Technique to simulate the flow in a Naturally Fractured Reservoir. This technique allowed to correctly capture the effects due to the fractures: a reduction in pressure and temperature in the flow through the fractures.

We also highlight here the speedup gain obtained with the use of the Preconditioned Conjugate Gradient, which is very important to save computational time when we have to use a grid refinement near the fractures, mainly when it is necessary to increase the number of fractures.

In the future, we intend to use our simulator in the investigation of the advanced recovery process using the static heating wells, to determine the best configurations resulting in increased production. As well as to study the effects of the number of fractures in the variation of the reservoir pressure and temperature fields, especially in the region near the producer well.

6. ACKNOWLEDGEMENTS

Authors gratefully thanks Rio de Janeiro State University, Coordination for the Improvement of Higher Education Personnel (CAPES) - Finance Code 001 and Rio de Janeiro Research Foundation (FAPERJ) for their support.

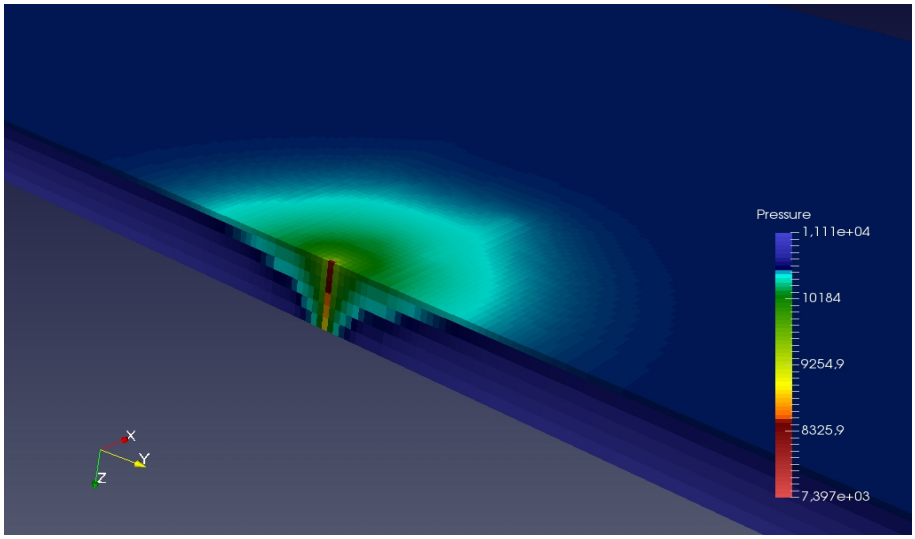

(a) Pressure distribution: yz-plane view.

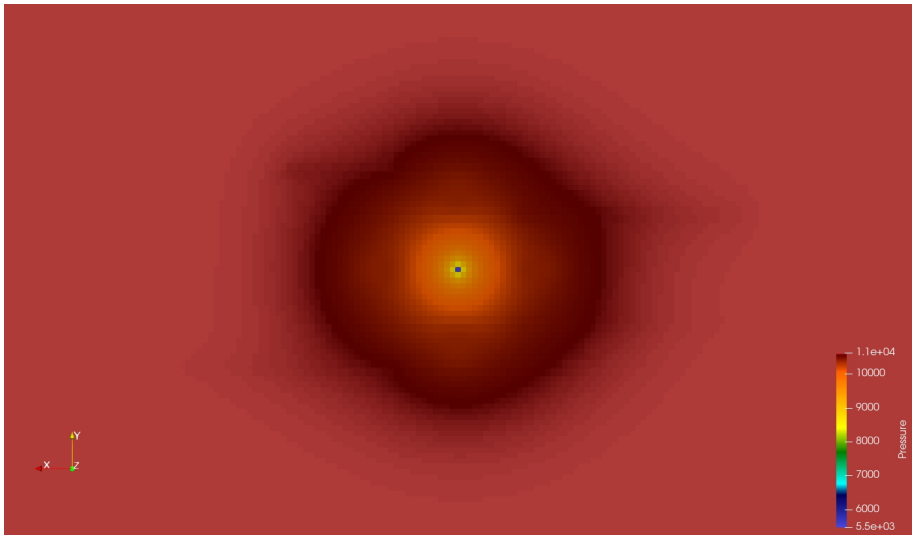

(b) Pressure distribution: xy-plane view

Figure 3. Pressure distribution along the reservoir for t_{max} equal to 600 days.

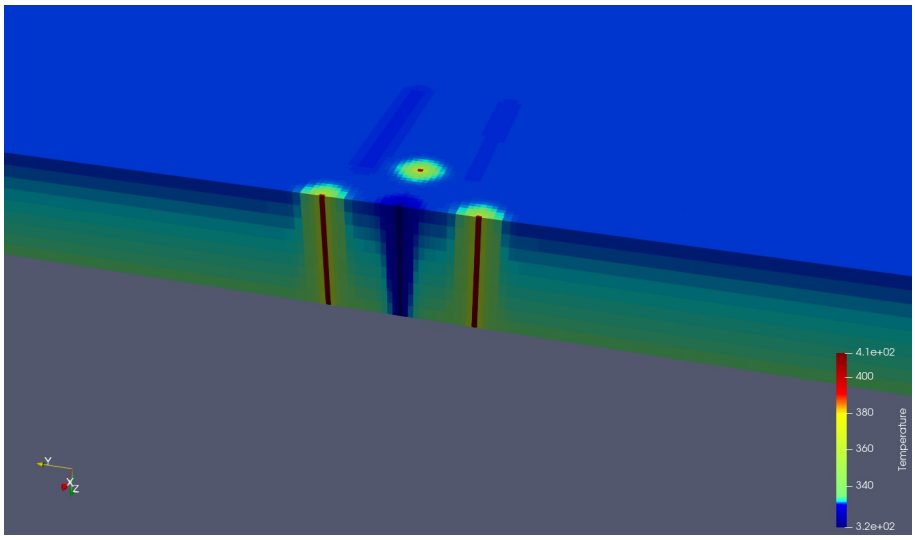

Figure 4. Three dimensional temperature distribution (yz-plane view) along the reservoir for t_{max} equal to 600 days.

7. REFERENCES

de Souza, G. and Souto, H.P.A., 2014. "Numerical reservoir simulation of naturally fractured reservoirs". In *Proceedings of the XXXV Iberian Latin-American Congress on Computational Methods in Engineering*. Fortaleza, CE, Brazil.

Dyrdah, J., 2014. *Thermal flow in fractured porous media and operator splitting*. Ph.D. thesis, Norwegian University of Science and Technology, Norway.

Ertekin, T., Abou-Kassem, J. and King, G., 2001. *Basic Applied Reservoir Simulation*. Richardson, USA: Society of Petroleum Engineers, Texas.

Ezeuko, C.C. and Gates, I.D., 2018. "Thermal oil recovery from fractured reservoirs: Energy and emissions intensities". *Energy*, Vol. 155, pp. 29–34.

Heringer, J.D.S., Debossam, J.G.S., de Souza, G. and Souto, H.P.A., 2019. "Numerical simulation of non-isothermal flow in oil reservoirs using a two-equation model". *Coupled Systems Mechanics*, Vol. 8, No. 2.

Jansen, G., 2018. *THERMAID: User Quick Start Guide v.1.01*. Swiss.

Lampe, V., 2013. *Modelling fluid flow and heat transport in fractured porous media*. Ph.D. thesis, University of Bergen, Norway.

Leveque, R.J., 2004. *Finite-Volume Methods for Hyperbolic Problems*. Ph.D. thesis, Cambridge.

Liu, Y., Liu, X., Hou, J., Li, H.A., Liu, Y. and Chen, Z., 2019. "Technical and economic feasibility of a novel heavy oil recovery method: Geothermal energy assisted heavy oil recovery". *Energy*, Vol. 181.

Manichand, R.N., 2002. *Análise do Desempenho do Aquecimento Eletromagnético na Recuperação de Reservatórios de Petróleo'*. Ph.D. thesis, Rio Grande do Norte State University, Brazil.

Mezon, C., Mourzenko, V.V., Thovert, J.F., Antoine, R., Fontaine, F., Finizola, A. and Adler, P.M., 2018. "Thermal convection in three-dimensional fractured porous media". *Physical Review E*, Vol. 97.

Moukalled, F., Mangani, L. and Darwish, M., 2016. *The Finite Volume Method in Computational Fluid Dynamics: An Advanced Introduction with OpenFOAM and Matlab*. Ph.D. thesis, Switzerland.

Moyne, C., Didierjean, S., Amaral Souto, H.P. and Silveira, O.T.D., 2000. "Thermal dispersion in porous media: one-equation model". *International Journal of Heat and Mass Transfer*, Vol. 43, No. 2.

Praditia, T., Helmig, R. and Hajibeygi, H., 2018. "Multiscale formulation for coupled flow-heat equations arising from single-phase flow in fractured geothermal reservoirs". *Computational Geosciences*, Vol. 22, No. 5.

Rosa, A., Carvalho, R. and Xavier, J., 2006. *Engenharia de reservató rios de petrÃşleo*. InterciÃłncia, Brazil.

Safari, M., Mohammadi, M. and Sedighi, M., 2017. "Effect of neglecting geothermal gradient on calculated oil recovery". *Journal of Applied Geophysics*, Vol. 29, No. 1, pp. 81–91.

Vennemo, S.B., 2016. *Multiscale Simulation of Thermal Flow in Porous Media*. Ph.D. thesis, Norwegian University of Science and Technology, Trondheim, Norway.

8. RESPONSIBILITY NOTICE

The authors, Juan Diego dos Santos Heringer, Paulo de Tarço Honório Jr., Grazione de Souza and Helio Pedro Amaral Souto, are the only responsible for the printed material included in this paper.